The Influence of Mesoscale Eddies on Coarsely Resolved Density: An Examination of Subgrid-Scale Parameterization

SARAH T. GILLE AND RUSS E. DAVIS

Physical Oceanography Research Division, Scripps Institution of Oceanography, La Jolla, California

(Manuscript received 9 June 1997, in final form 1 June 1998)

ABSTRACT

Coarse-resolution numerical models of ocean circulation rely on parameterizations of unresolved mesoscale eddy effects. In order to investigate the role of eddy-flux divergences in the density equation, the GFDL Modular Ocean Model (MOM) has been configured as a simple flat-bottomed channel model with sufficient resolution to represent mesoscale eddies. Eady-type baroclinic instability and a wind-forced channel have been considered. As an analog to the large-scale components addressed by low-resolution models, the influence of eddy fluxes on the zonal-mean density field was evaluated. Results show that eddy-flux divergences are larger than mean-flux divergences. The effect of mesoscale eddies on the mean density field is often hypothesized to take an advective form that conserves mean density so that eddy effects are adiabatic in the zonal mean. However, in both of the examples studied a significant component of the mesoscale eddy effect on the zonal mean is diabatic and makes mean density nonconservative. The associated diapycnal fluxes result from zonally averaging terms representing processes that are locally adiabatic.

Subgrid-scale parameterizations (such as eddy diffusion) represent the unresolved eddy-flux divergence as a function of the resolved density field. The authors computed optimal coefficients for a variety of parameterizations and evaluated their skill. When the model output is time-averaged, quasi-adiabatic parameterizations, such as the one proposed by Gent and McWilliams, are able to explain as much as 43% of the mean-squared eddy-flux divergence. However, for shorter averaging periods or instantaneous snapshots, even for the spatially averaged model fields, parameterization skill drops.

1. Introduction

Numerical models of ocean circulation must represent large-scale oceanic flows such as western boundary currents and the circumpolar current. In observations and in high-resolution numerical models, these currents are intimately bound to the mesoscale eddy field, which can transfer momentum vertically or horizontally. On the other hand, models of decadal to millennial climate variations are constrained by computational limitations to resolutions coarser than eddy length scales. In these models eddy effects must be parameterized.

The search for realistic parameterizations of mesoscale eddy effects has produced a number of recent studies (e.g., Gent and McWilliams 1990; Danabasoglu et al. 1994; Tandon and Garrett 1996; Visbeck et al. 1997; McDougall and McIntosh 1996; Gent and McWilliams 1996; Griffies 1998) that have focused primarily on the theoretical requirements for good mesoscale parameterizations or have described coarse-resolution fields obtained using a variety of parameterizations. The present study employs a different approach by, instead, running idealized model scenarios at a resolution high enough to resolve the mesoscale. We then examine the actual role of mesoscale eddies. Can they be represented using an adiabatic form as suggested by Gent and McWilliams (1990), and more generally, do any of the standard eddy parameterizations duplicate the eddy physics?

Because the hydrostatic and geostrophic balances dominate ocean dynamics at length scales larger than the mesoscale, ocean circulation depends strongly on evolution of the density field. Here we examine density, ρ, which is a dynamically active tracer governed by

$$\frac{D\rho}{Dt} = \frac{\partial \rho}{\partial t} + \mathbf{u} \cdot \boldsymbol{\nabla} \rho = R(\rho), \tag{1}$$

where $\mathbf{u}$ is the velocity, $R(\rho)$ represents molecular diffusive processes that are negligible on the scales that we consider, and density sources are not included. The advection embodied in the substantial derivative $D\rho/Dt$ is conservative. Water at any given location can move, and isopycnals may shift, but water parcels do not exchange density with the environment, so that the volume of water in any density class remains constant. In this sense $D\rho/Dt$ will be termed adiabatic, although by strict

Corresponding author address: Dr. Sarah Gille, Department of Earth System Science, University of California, Irvine, Irvine, CA 92697-3100.
E-mail: sgille@uci.edu

definitions adiabatic processes should conserve heat rather than density. The operator $R(\rho)$ represents diabatic processes that do alter the properties of individual water parcels. In the problems considered here $R(\rho)$ is small.

If (1) is locally smoothed in space to represent the low-resolution ρ field, as in a climate model, it becomes

$$\frac{\partial \hat{\rho}}{\partial t} + \hat{\mathbf{u}} \cdot \nabla \hat{\rho} + S(\mathbf{u}, \rho) = \widehat{R(\rho)}, \tag{2}$$

where

$$S(\mathbf{u}, \rho) = \widehat{\mathbf{u} \cdot \nabla \rho} - \hat{\mathbf{u}} \cdot \nabla \hat{\rho}. \tag{3}$$

The caret represents a local spatial and/or temporal filtering operator and deviations from the smoothed quantities will be denoted by primed values, $\mathbf{u}'$ and ρ'. In a model without the resolution to compute eddy-scale deviations, the advective terms in $S(\mathbf{u}, \rho)$ must be parameterized. The processes resolved by a coarse-resolution model represent oceanwide advection, while unresolved processes are typified by mesoscale eddies, which are often linked to baroclinic instability. Thus, a satisfactory subgrid-scale parameterization of oceanic mixing must imitate the mesoscale effects of eddies, such as those formed through instability.

Past work on parameterizations of small scales for climate modeling has relied on two hypotheses that we examine. The first hypothesis, specifically suggested by Gent and McWilliams (1990), is that evolution of the filtered large-scale density $\hat{\rho}$ should be adiabatic. Thus, they neglected eddy fluxes through smoothed isopycnals and represented all significant eddy effects on the large-scale tracer as an adiabatic advection process $\mathbf{u}^* \cdot \nabla \hat{\rho}$, where $\mathbf{u}^*$ is a parameterized, nondivergent velocity. In this study we examine how well $\mathbf{u}^* \cdot \nabla \hat{\rho}$ describes $S(\mathbf{u}, \rho)$. We find that eddy-induced advection, which is adiabatic in the high-resolution model, will appear diabatic if we examine only the components resolved by coarse-resolution models. These effective diabatic processes are responsible for significant diapycnal eddy fluxes.

The second hypothesis examined is that the eddy-flux terms have a simple functional relationship to $\hat{\rho}$ and its spatial derivatives so that $S(\mathbf{u}, \rho) = S(\hat{\rho})$. The physical rationale for such parameterizations and the behavior of the resultant density evolution equation require a net downgradient transfer of density, although studies of baroclinic instability indicate that density may be transferred upgradient as well. The results shown here indicate that standard parameterizations do not generally describe the instantaneous effects of $S(\mathbf{u}, \rho)$, though the parameterizations are more successful when results are time averaged.

These conclusions are based on using high-resolution model runs to analyze the advective terms represented by $S(\mathbf{u}, \rho)$. The model is the Geophysical Fluid Dynamics Laboratory (GFDL) Modular Ocean Model (MOM) (Pacanowski 1995), which is discussed in section 2. MOM was adapted for two physical scenarios outlined in section 3. The first is the simple example of baroclinic instability outlined by Eady (1949), and the second is a wind-forced channel model. Both cases are implemented in a reentrant channel on the f plane, and in both an alongchannel (zonal) average is used to define the low-resolution fields $\hat{\mathbf{u}}$ and $\hat{\rho}$. Section 4 explores the influence of the advective terms in the zonally averaged model output and in particular evaluates whether the eddy-flux divergence can be treated as an adiabatic advection of the zonal-mean density. In section 5, we attempt to parameterize the eddy-flux divergence terms from the high-resolution run in terms of coarse-resolution model variables. Section 6 summarizes the results of this study.

2. Numerical model

The GFDL MOM is a primitive equation model that has been used extensively to investigate ocean circulation, including studies of the effects of the GM90 parameterization on coarse-resolution climate models (Danabasoglu et al. 1994; Danabasoglu and McWilliams 1995; McWilliams et al. 1996). The same model is also the heart of several near-eddy-resolving simulations of modern ocean circulation (FRAM Group 1991; Semtner and Chervin 1992).

The basic model physics and algorithms have been summarized by Semtner (1986) and Pacanowski (1995). Density evolution is described by a discretized form of (1) with $R(\rho)$ represented by horizontal diffusion, vertical diffusion, and convective adjustment. For this study, the model domain is a reentrant channel on the f plane, at 50°S, extending approximately 2300 km in the zonal direction and 1150 km in the meridional direction. Zonal and meridional grid spacings are 17.7 km. A single-constituent equation of state is used in which density depends linearly on temperature. In this formulation, constraining tracer diffusion to take place along isopycnals, as formulated by Cox (1987), is equivalent to allowing no diffusion whatsoever. Table 1 summarizes key model parameters.

Horizontal and vertical viscosity and diffusion coefficients are adjusted to the minimum values needed to maintain model stability so that the mesoscale features of interest are minimally influenced by the parameterized processes. Horizontal viscosity ν_H is 10 $m^2\ s^{-1}$ in the Eady case and 1×10^3 $m^2\ s^{-1}$ in the wind-forced case. The diffusion coefficient κ_H is 0.2 $m^2\ s^{-1}$. For the Eady case, these values are slightly smaller than the stability criterion values suggested by Bryan et al. (1975), who showed that to prevent grid-scale instabilities the viscosity should exceed a minimum value, $\nu_{H,\text{crit}} > |U|\Delta/2$, where U is the background horizontal velocity and Δ is the grid spacing. For this Eady problem, $\nu_{H,\text{crit}} = 4.1 \times 10^2$ $m^2\ s^{-1}$. However, Bryan et al. (1975) noted that, for cases with smooth

TABLE 1. Parameters applied to the Eady instability in the middle column and the wind-forced channel in the right column. Some of the parameters define the initial conditions for the Eady background state and do not apply to the wind-forced case.

Parameter	Eady instability	Wind-forced
f	1.12×10^{-4} s^{-1}	1.12×10^{-4} s^{-1}
L_x	2287 km = 32°	2287 km
L_y	1143 km = 16° × cos(50°)	1143 km
D	1500 m	5700 m
n_{levels}	15	15
ν_H	10 m^2 s^{-1}	1000 m^2 s^{-1}
κ_H	0.2 m^2 s^{-1}	0.2 m^2 s^{-1}
$\nu\upsilon$	0 m^2 s^{-1}	1×10^{-4} m^2 s^{-1}
$\kappa\upsilon$	0 m^2 s^{-1}	1×10^{-5} m^2 s^{-1}
ncon	4	4
α	4.67×10^{-5} s^{-1}	
γ	6.67×10^{-4} kg m^{-4}	
ρ_o	1000 kg m^{-3}	
H	750 m	

inflow (such as the Eady problem), smaller viscosities may be acceptable. They also indicated that diffusion may be several orders of magnitude smaller than viscosity. Numerical viscosity and numerical diffusion are the same: $\nu_{H,\text{num}} = \kappa_{H,\text{num}} = k\tilde{U}\Delta^2/4$, where k is the wavenumber, and $\tilde{U}$ the Fourier transform of U. Because the viscosity and diffusion coefficients are set to be small, at high wavenumbers numerical viscosity and diffusion may exceed the parameterized coefficients. In practical terms, this means that numerical viscosity and diffusion may attenuate energies in the upper half of the wavenumber spectrum, particularly for the Eady problem.

Since vertical diffusion and viscosity predominantly represent diapycnal effects, which are believed to be minor in much of the ocean interior, they are set to be smaller than their horizontal counterparts. For the Eady problem, where energetics are important, vertical diffusion and viscosity coefficients are set to zero in order to minimize potential energy changes during the run. For the wind-forced case, $\nu_\upsilon = 1 \times 10^{-4}$ m^2 s^{-1} and $\kappa_\upsilon = 1 \times 10^{-5}$ m^2 s^{-1}.

Standard convective adjustment is used to mix the water column vertically where it is unstably stratified. Four convective passes through the water column are carried out at each time step. Convection is a minor process in the Eady instability, but it is important in the wind-forced model.

For this study, only examples on the f plane are considered. Without β there are no Rossby waves, so the slow spinup timescales associated with Rossby waves are not a concern. While instabilities that rely on a background vorticity gradient may exhibit some behaviors different from those found on an f plane, observed oceanic instabilities can closely resemble Eady instabilities, which occur on the f plane. For example, Samelson (1993) has noted that mixed layer fronts, such as those observed in the FASINEX experiment, are unstable with growth rates similar to the Eady model predictions.

Since the goals of this study are to observe how mesoscale processes influence coarse-resolution processes, the model is run with sufficient resolution to permit baroclinic instability. The results are then averaged, as suggested by (2), to duplicate the coarse resolution of a typical climate model, and the influence of the unresolved eddy terms on the resolved mean terms is examined. Determining the appropriate form for the filtering operation $\hat{\cdot}$ is important. Since we use a flat-bottomed domain, there is no intrinsic difference between points at fixed depth and latitude anywhere along the length of the channel, and we adopt a zonal average as the filtering operation. This simplifies (3) to

$$S(\mathbf{u}, \rho) = \overline{\mathbf{u}' \cdot \nabla\rho'}, \tag{4}$$

where the overbar represents the zonal mean. Thus, we need only consider how the mean fields (e.g., $\overline{\rho}$) are influenced by deviations from the zonal means (e.g., $\overline{\upsilon'\rho'}$).

Some recent investigations have advocated investigating eddy effects by averaging thickness fluxes along isopycnals rather than density fluxes at fixed depth as used here. While isopycnally averaged fluxes might provide a clearer picture of the physical processes, any resulting parameterization would need to be converted to fixed-depth averages before being implemented in z-coordinate models such as MOM. Converting z-coordinate model output to isopycnal coordinates introduces numerical interpolation errors into the flux divergence computation. In cases where stratification is sufficiently uniform to make interpolation reliable, there is often no advantage to working on isopycnal surfaces because the z-coordinate density flux $\overline{\upsilon'\rho'}$ differs only by a stratification term from the thickness flux on an isopycnal η, which can be expressed to leading order as $\overline{\upsilon(\eta)'\Delta\eta'} \approx \overline{\upsilon(z)'\rho(z)'dz/d\rho}$. For these reasons we have restricted our attention to the z-average fluxes, which are natural to the model analyzed.

3. Model formulations

a. The Eady problem

The Eady model (Eady 1949) exhibits one of the clearest examples of baroclinic instability, and the basic physics underlying this instability has been carefully presented by a number of authors (Gill 1982; Pedlosky 1987). Because of its simplicity, it offers a direct means to examine mesoscale eddy processes. A signature of baroclinic instability is available potential energy associated with tilting isopycnals feeding a growing disturbance. Since the Eady instability grows rapidly at a dominant wavenumber, it allows us to examine how unresolved eddies influence coarse-resolution (zonally averaged) flow on timescales too short to allow averaging of a broad spectrum of mesoscale processes. Our analysis will indicate that classic frictionless Eady instability is effectively unparameterizable because it cannot achieve a steady state.

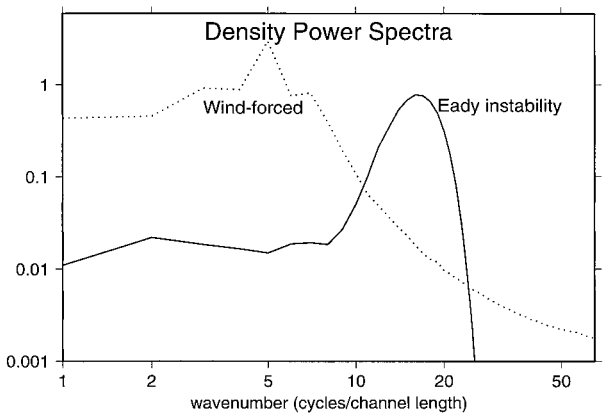

FIG. 1. Zonal wavenumber spectrum for density averaged vertically and meridionally in $kg^2\ m^{-6}$. The wind-forced spectrum has been divided by 100, and for the Eady case, the spectrum is an average of 15 separate realizations. The analyzed time periods are days 110 to 135 at 5-day intervals for the Eady case and days 3000 to 7000 at quarter-day intervals for the wind-forced case. For the Eady instability, the most unstable mode is between 16 and 17 wavelengths per channel length, while the most energetic wind-forced mode is 5 wavelengths per channel. Both are are well resolved by the 128-point zonal grid used in this study.

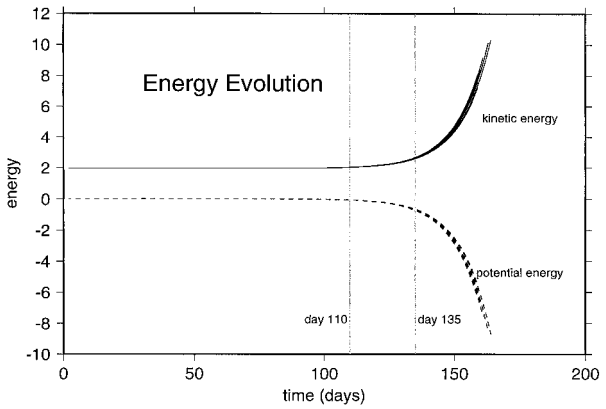

FIG. 2. Mean kinetic and potential energy (in $cm^2\ s^{-2}$) for the Eady problem run at quarter-degree resolution as a function of time (in days) from the beginning of the model run. The initial value of potential energy ($872\ cm^2\ s^{-2}$) is removed to better illustrate the transfer of potential energy to kinetic energy. The time period analyzed in this paper is delineated by vertical gray lines indicating days 110 and 135, when kinetic energy has increased between 5% and 50% above its initial value.

In the Eady model, rigid horizontal boundaries are imposed at the top and bottom of the domain of depth $2H$. The initial density field is

$$\rho(x, y, z) = \rho_0\left[1 - \gamma z + \frac{f\alpha}{g}y\right], \tag{5}$$

where the vertical and horizontal stratifications, γ and α, and Coriolis parameter f are all constant, as is the Brunt–Väisälä frequency $N^2 = g\gamma$. The initial flow is in geostrophic balance, varies only with depth, and has shear $\partial u/\partial z = \alpha$.

The growth rate of a perturbation with zonal wavenumber k and meridional wavenumber l is

$$\sigma = kc_i = \alpha\left\{\left[H\tanh\left(\frac{H}{H_R}\right) - H_R\right]\left[H\coth\left(\frac{H}{H_R}\right) - H_R\right]\right\}^{1/2}, \tag{6}$$

where $H_R = f/N\kappa$ and $\kappa = k^2 + l^2$ (Gill 1982). In our numerical reentrant channel the lowest mode is approximately $l = \pi/L_y$ in which case $\sigma_{\max} = 0.3093\alpha f/N$, which occurs when $k = [(0.8038\, f/(NH))^2 - (\pi/L_y)^2]^{1/2}$.

In this numerical implementation of the Eady problem, the model ocean is 1500 m deep and is divided into 15 levels, each 100 m thick. Other parameters are listed in Table 1. The most unstable mode is predicted to be 16.9 wavelengths per channel length. As indicated by the solid line in Fig. 1, this mode is highly energetic and is well resolved by the 128-point zonal grid.

Numerical solutions to the Eady problem were considered by Williams (1971), who analyzed flow in an annulus, an experiment akin to what might be set up in a laboratory rotating tank. His situation differed slightly from the Eady idealization because frictional boundaries were included at $y = 0$ and $y = L_y$. The resulting instability growth was constrained by friction within the boundary layers. In contrast, in this study, free-slip boundary conditions are used on the sidewalls and on the upper and lower boundaries, and the instability grows without bound. Free-slip boundary conditions are obtained by fixing the derivative $\partial u/\partial y$ to be zero on the northern and southern boundaries. In addition, the term $\partial^2\rho/\partial y^2$ is also set to zero at the boundaries to maintain the geostrophic balance. As indicated in Fig. 2, potential energy decreases over time, as it is converted into kinetic energy. One might suppose that with the right initial parameters, the background stratification could be made to evolve until the isopycnals were flattened and all the initial available potential energy was converted to kinetic energy. This does not occur with the minimal explicit damping used here. Our three-dimensional code behaves much like the two-dimensional Eady instability analyzed by Garner et al. (1992). Because the flow is in approximately thermal wind balance, as potential energy is converted to eddy kinetic energy, the isopycnals steepen and there is a progression toward small scales. Since MOM was implemented with free-slip boundary conditions and no sidewall friction, even if the flow begins with little available potential energy, the growing instability generates progressively narrower structures that eventually vary too rapidly to be represented numerically.

Instabilities in the real ocean do not grow without bound, but the early growth stages of oceanic instability may be represented by the early growth of the Eady instability. Thus, we analyze the Eady problem results

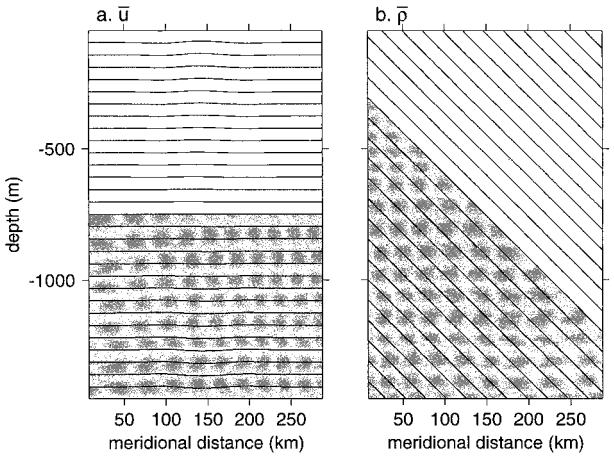

FIG. 3. Cross sections showing zonal and time averages of variables from day 110 to 135 at 5-day intervals for the evolving Eady instability. Panels indicate (a) the zonal velocity $\overline{u}$ with contour interval 2.2×10^{-3}m s^{-1} and (b) the density anomaly $\delta\overline{\rho}$ with contour interval 5.2×10^{-4} kg m^{-3} and density defined as $\rho_0 - \delta\overline{\rho}$. Gray regions correspond to negative values. Meridional distance is measured from south to north, with f negative. Readers who prefer to think about systems with positive f should interpret meridional distance as extending from north to south.

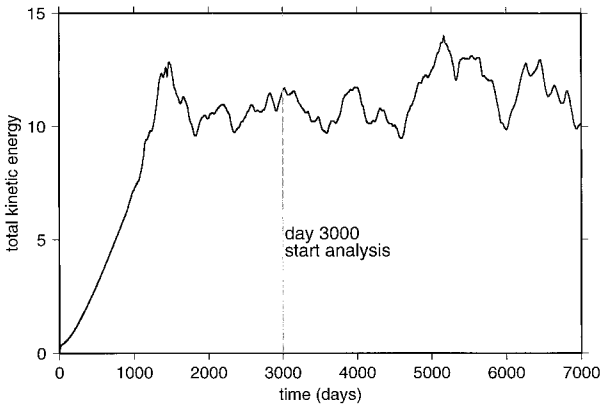

FIG. 4. Mean kinetic energy (in cm^2 s^{-2}) of wind-forced channel model, as a function of time (in days) from the beginning of the model run. Output is analyzed from day 3000 to 7000 at quarter-day intervals.

when the total kinetic energy has increased between 5% and 50% above the initial kinetic energy level, as indicated in Fig. 2. Figure 3 shows at full resolution the zonal averages of velocity u and density ρ, time-averaged over this window and over 15 model realizations. The density field in Fig. 3b has not changed perceptibly from its initial condition defined by (5). The zonal velocity in Fig. 3a shows only slight perturbations from its initial state.

b. Wind-forced reentrant channel

In addition to the unconditionally unstable Eady problem, a wind-forced reentrant channel on the f plane is considered. Surface wind forcing is constant in time and eastward, with a Gaussian structure centered in the channel and an e-folding scale one-sixth the channel width. In contrast to the Eady case, no-slip boundary conditions are used on the northern and southern walls, a frictional drag coefficient is applied on the bottom boundary, and the boundary drag removes momentum input by the wind. The constant channel depth of 5700 m is divided into 15 levels with thicknesses varying from 30 m at the surface to 840 m at the bottom. The vertical structure matches that used in climate simulations carried out with MOM, and the use of a deep channel prevents bottom friction from controlling the ocean response to wind forcing. The initial density field is set to have a realistic vertical structure based on fits to observations by Pacanowski (1995).

The model is spun up from an initial resting state. Kinetic energy reaches equilibrium after about 1500 model days, as shown in Fig. 4. For comparison, the spinup timescale due to a frictional surface Ekman layer $2H/\sqrt{2\nu_v f}$ (Pedlosky 1987) is estimated to be 450 days. Thus, the equilibrium energy appears to represent a state that has spun up the surface Ekman layer.

The wind-forced flow in a channel evolves into a strong zonal-velocity jet (Fig. 5a) with correspondingly sloping isotherms (Fig. 5b). The most energetic zonal wavenumber is five wavelengths per channel, as indicated in Fig. 1.

4. Examining the role of eddies

In this section we examine how eddies affect the two model runs described above. The analysis is based on the transformed Eulerian-mean equations originally de-

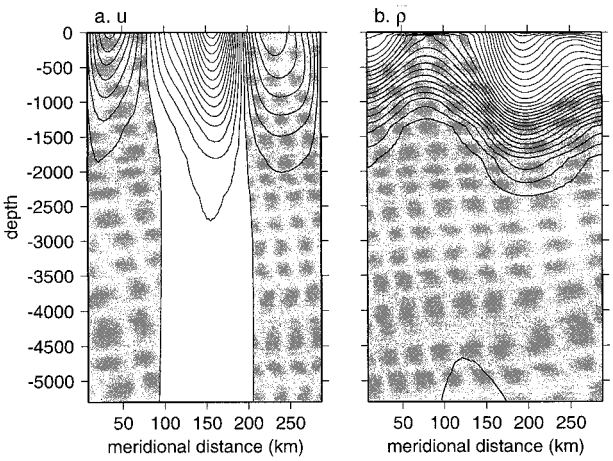

FIG. 5. Cross sections showing zonal and time averages of variables from day 3000 to day 7000 at quarter-day increments for the evolving wind-forced channel at quarter-degree resolution. Panels indicate (a) the zonal velocity $\overline{u}$ with contour intervals of 1.3×10^{-2} m s^{-1} and (b) the density anomaly $\delta\overline{\rho}$ with contour interval 2×10^{-2} kg m^{-3} and density defined as $\rho_0 - \delta\overline{\rho}$. Gray regions correspond to negative values.

veloped for the atmosphere (see Andrews et al. 1987) and adopted by Gent and McWilliams (1996) and by Tandon and Garrett (1996) to interpret oceanic eddy effects. The power of this approach is that it clarifies how eddies can have two rather distinct roles in the resolved-scale dynamics: an eddy-induced advection and an eddy flux through mean isopycnals. In the transformed Eulerian-mean equations, the tracer balances (2) and (4) are written as

$$\frac{D^*\overline{\rho}}{Dt} = \frac{\partial\overline{\rho}}{\partial t} + \overline{\mathbf{U}}\cdot\nabla\overline{\rho} = -G_z + \overline{R(\rho)}, \tag{7}$$

$$\overline{\mathbf{U}} = \overline{\mathbf{u}} + \mathbf{u}^* = \overline{\mathbf{u}} + \left[-\left(\frac{\overline{u'\rho'}}{\overline{\rho}_z}\right)_z, -\left(\frac{\overline{v'\rho'}}{\overline{\rho}_z}\right)_z, \left(\frac{\overline{u'\rho'}}{\overline{\rho}_z}\right)_x + \left(\frac{\overline{v'\rho'}}{\overline{\rho}_z}\right)_y\right], \tag{8}$$

$$G = \frac{1}{\overline{\rho}_z}\nabla\overline{\rho}\cdot\overline{\mathbf{u}'\rho'}, \tag{9}$$

where G_z is the vertical derivative of G.

The eddy-induced transport velocity $\mathbf{u}^*$ is nondivergent, and the sum of $\overline{\mathbf{u}} + \mathbf{u}^*$ is the residual mean circulation $\overline{\mathbf{U}}$. The term G depends on the component of the eddy flux that is diapycnal relative to the mean, that is, the flux through mean isopycnals. In this form of the Eulerian-mean equations, the eddy terms (4) have been separated into two components:

$$S(\mathbf{u}, \rho) = \overline{\mathbf{u}'\cdot\nabla\rho'} = \mathbf{u}^*\cdot\nabla\overline{\rho} + G_z. \tag{10}$$

The eddy-induced total derivative D^*/Dt, representing advection of $\overline{\rho}$ by $\overline{\mathbf{U}}$, cannot change the volume of water within any given filtered density range ($\rho_1 < \overline{\rho} < \rho_2$). The term G_z, on the other hand, is the eddy-flux divergence in the ''mean diapycnal'' direction; although locally density advection is confined within isopycnal surfaces, relative to $\overline{\rho}$ G_z can produce or destroy filtered density. In this section, we will use the term ''diabatic'' to refer to processes that are diabatic in zonally averaged coordinates (though they are locally adiabatic), ''adiabatic'' to refer to processes that neither create nor destroy zonal-mean density, and ''diapycnal'' to refer to motions across zonal-mean isopycnals. Here G differs from the mean diapycnal component of the eddy flux only by the factor $\overline{\rho}_z/|\nabla\rho|$, which is nearly unity.

The merit of the transformed Eulerian-mean equations, originally developed by Andrews and McIntyre (1976) to describe the effect of atmospheric waves, is the separation of eddy effects into the advecting component $\mathbf{u}^*$ in (8) and the diabatic component G_z of (9). There are, of course, myriad ways to partition $S(\mathbf{u}, \rho)$ into adiabatic and diabatic components, but the particular form selected is unique in associating all the effects of G_z with the diapycnal eddy flux, which is believed to be small in the atmosphere and ocean.

Although the processes due to G_z are strictly diapycnal, it does not follow that the eddy transport velocity $\mathbf{u}^*$ advects tracers along isopycnals. In many quasi-equilibrium scenarios in which the low-resolution density field is approximately steady the effects of diapycnal advection by the Eulerian-mean $\overline{\mathbf{u}}$ and eddy-induced transport velocity $\mathbf{u}^*$ compensate to make $D^*\overline{\rho}/Dt$ small. If the eddy-induced and Eulerian-mean advection were directed along isopycnals, then the meridional overturning streamfunctions $\overline{\psi}$ and ψ^* corresponding to $\overline{\mathbf{u}}$ and $\mathbf{u}^*$ would be parallel to isopycnals. Figures 6a,b and 7a,b show streamfunctions for the Eady and wind-forced cases, respectively. Isopycnals are superimposed in dotted lines. In neither case is $\overline{\psi}$ or ψ^* parallel to isopycnals. In the wind-forced case, which is in quasi equilibrium, the two processes tend to compensate to minimize net diapycnal advection.

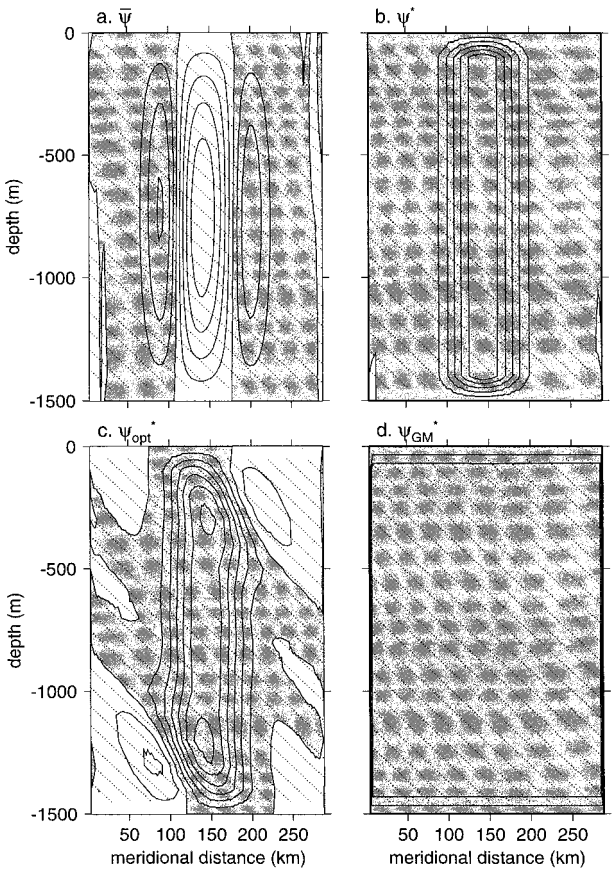

FIG. 6. Meridional streamfunctions ψ for the Eady instability case represented with solid contours and shading, calculated from zonally and time-averaged velocity and density fields, with $v = -\psi_z$ and $w = \psi_y$. Dotted contours indicate isopycnals from Fig. 3b. Panels show (a) $\overline{\psi}$ corresponding to the zonal-mean velocity $\overline{\mathbf{u}}$ (with contour interval 1.67×10^{-4} m^2 s^{-1}), (b) $\psi^* = \overline{v'\rho'}/\overline{\rho}_z$ corresponding to $\mathbf{u}^*$ as defined in (8) (with contour interval 1.67×10^{-2} m^2 s^{-1}), (c) ψ^*_{opt} (with contour interval 1.67×10^{-2} m^2 s^{-1}) found by least squares fitting $\mathbf{u}^*_{opt}$ to minimize G_z (see text), and (d) $\psi_{GM} = -K_i\overline{\rho}_y/\overline{\rho}_z$, the parameterized streamfunction suggested by GM90, with $K_i = 60$ m^2 s^{-1} and contour interval 1.67×10^{-2} m^2 s^{-1}. Negative streamfunction values are shaded gray, and by definition the streamfunctions are zero on the boundaries.

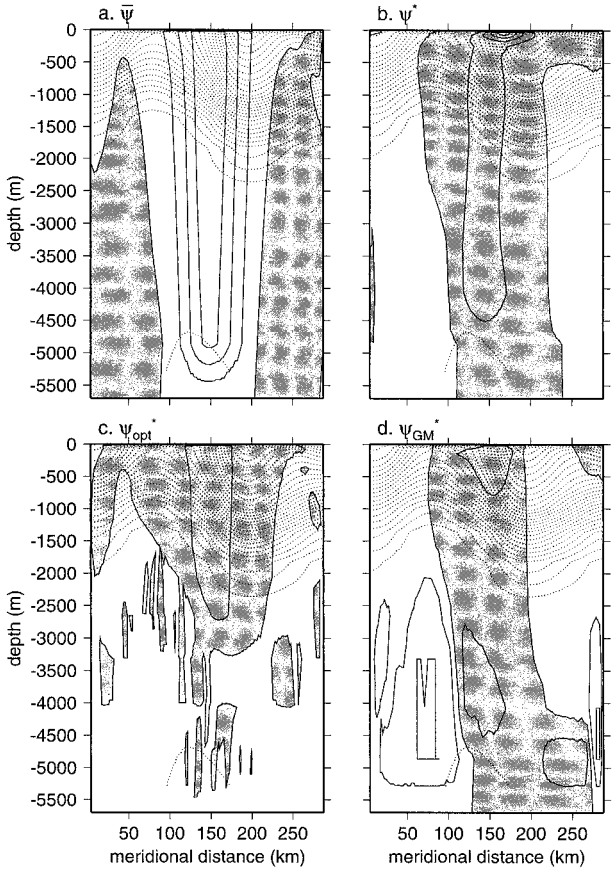

FIG. 7. Meridional streamfunctions ψ for the wind-forced case, calculated from zonally and time-averaged velocity and density fields (solid contours and shading), as in Fig. 6. Dotted contours indicate isopycnals from Fig. 5b. Panels show (a) $\overline{\psi}$ (with contour interval 0.5 m^2 s^{-1}), (b) $\psi^* = \overline{v'\rho'}/\overline{\rho}_z$ (with contour interval 1.25 m^2 s^{-1}), (c) ψ^*_{opt} (with contour interval 1.25 m^2 s^{-1}; values within 0.01 m^2 s^{-1} of zero are plotted as positive values), and (d) $\psi_{GM} = -K_I\overline{\rho}_y/\overline{\rho}_z$, (with $K_I = 2.5 \times 10^2$ m^2 s^{-1} and contour interval 1.25 m^2 s^{-1}).

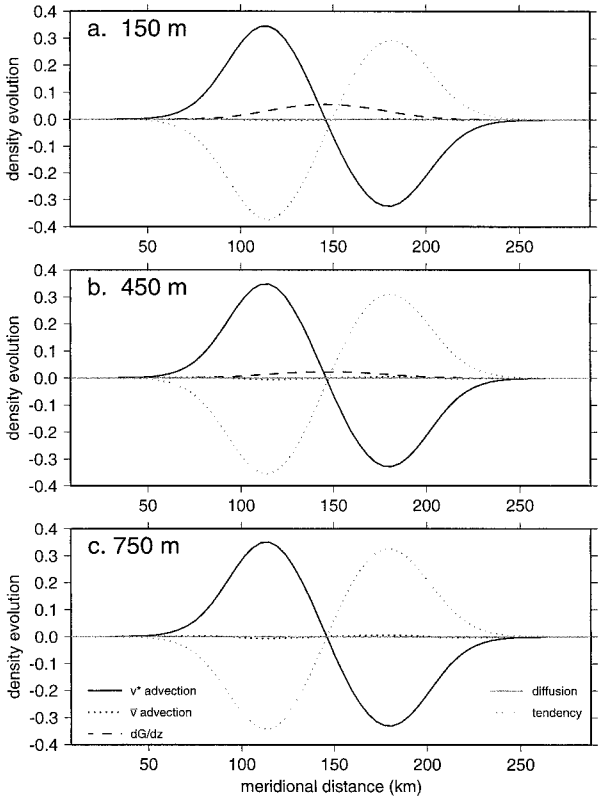

FIG. 8. Eady model density balance (in kg m^{-3} s^{-1} $\times$ 10^6) averaged over 15 model realizations, zonally and temporally at 5-day intervals from day 110 to 135 for (a) level 2, (b) level 5, and (c) level 8. Because of the vertical symmetry of the Eady problem, balances below 750 m are similar to those above 750 m. The terms from the density balance (7) are eddy-induced advection $v^*\overline{\rho}_y + w^*\overline{\rho}_z$ (black solid line); mean advection $\overline{v}\,\overline{\rho}_y + \overline{w}\,\overline{\rho}_z$ (black dotted line); G_z (black dashed line); negative diffusion $-\kappa_H\overline{\rho}_{yy} - \kappa_v\overline{\rho}_{zz}$ (gray solid line); and density tendency $\partial\overline{\rho}/\partial t$ (gray dotted line).

The terms in the density balance equation (7) are shown at three depths for the Eady case in Fig. 8 and for the wind-forced case in Fig. 9.

At all depths in the Eady instability case, the dominant balance is between density advection due to eddy effects ($\mathbf{u}^* \cdot \nabla\overline{\rho}$) and the time evolution ($\partial\overline{\rho}/\partial t$): G_z is the next largest term, substantially exceeding advection by the Eulerian-mean velocity. This suggests that G_z may be important when Eady instabilities are growing. To test the role of G_z, the Eady instability scenario was rerun with an additional fictitious, zonally invariant buoyancy source that exactly cancelled the zonally averaged G_z in the density equation. In this run the kinetic energy evolved as in the original case, but potential energy remained nearly constant. In addition, the wavenumber spectral peak was broader than what is shown in Fig. 1 and was less clearly dominated by the predicted most unstable mode. This shows that the small but significant values of G_z seen in Fig. 8 play a critical role in the growth of Eady-type instability.

At the wind-forced case's deeper levels (Figs. 9b,c) the advective effects due to mesoscale eddies ($\mathbf{u}^*$) roughly balance advection by the Eulerian-mean velocity ($\mathbf{u}$). This is analogous to the Ferrel cells in the atmosphere (Plumb and Mahlman 1987) and the Southern Ocean Deacon cell (Döös and Webb 1994) that are evident when the mean circulation is averaged in z coordinates but diminish when eddy effects are considered by averaging in pressure or density coordinates. The next most important contribution is from G_z. Nearer the top of the model domain (Fig. 9a) eddy advection, represented by $v^*\overline{\rho}_y + w^*\overline{\rho}_z$, is balanced primarily by G_z, while mean-flow advection plays a comparatively small role.

Since G_z is nonzero in both model cases considered, even a perfect parameterization of $\mathbf{u}^* \cdot \nabla\overline{\rho}$ alone may be inadequate, and parameterization of G may be required. Andrews and McIntyre (1976) based their ne-

glect of the role of G_z on analysis of a linearized balance equation for density variance $\overline{\rho'^2}$ in which the diapycnal flux appears to work against the mean gradient $\nabla\overline{\rho}$ to produce variance. The full variance budget, obtained by multiplying the ρ' evolution equation by ρ' and averaging zonally, is

$$\overline{\mathbf{u}'\rho'} \cdot \nabla\overline{\rho} = -\frac{1}{2}\frac{\partial\overline{\rho'^2}}{\partial t} - \frac{\overline{\mathbf{u}} \cdot \nabla\overline{\rho'^2}}{2} - \frac{\nabla \cdot \overline{\mathbf{u}'\rho'^2}}{2} + \kappa_H\overline{\rho'\rho'_{yy}} + \kappa_v\overline{\rho'\rho'_{zz}} + \overline{C(\rho)\rho'} = G\overline{\rho}_z, \tag{11}$$

where the diffusive processes $R(\rho)$ are here expressed as they are used in the numerical model, as horizontal and vertical diffusion and convective adjustment $C(\rho)$.

In the case of the linearizable wave motions considered by Andrews and McIntyre (1976), time change of variance was the dominant term on the right of (11). Alternatively, McDougall and McIntosh (1996) proposed that within the oceanic general circulation advection by the mean flow, $\overline{\mathbf{u}} \cdot \nabla\overline{\rho'^2}$, would dominate. Many observational inferences of the diapycnal flux are based on the Osborn–Cox model (Osborn and Cox 1972), which posits an approximate balance between production and the dissipation terms. This dissipation can be expressed by manipulating the terms involving κ_H and κ_v in (11) to yield a positive quantity representing dissipation of variance by explicit diffusion plus a divergence term that is generally small. As discussed by Davis (1994), hypotheses such as these depend on both the physical circumstances being studied (atmospheric waves versus oceanic fine scales) and the way fluctuations like ρ' are separated from mean or resolved components like $\overline{\rho}$. The Osborn–Cox model, for example, implicitly puts internal waves in the resolved field, whereas in the present model only the zonal mean passes through the averaging operation. Davis (1994) suggested that the turbulent flux of variance, $\overline{\mathbf{u}'\rho'^2}$, may become important in problems where the fluctuating field spans a broad range of scales and terms of very different scale are involved in the average triple product. Thus, past studies have reached no consensus about predicting the relative sizes of the terms in (11).

In light of the foregoing discussion, it is perhaps not surprising that our model runs show no simple description of the variance budget that could serve as a basis for parameterizing G. The terms represented in (11) are shown in Fig. 10 for the Eady instability case and in ig. 11 for the wind-forced model. In the Eady case, the system is not in steady state, and the time-dependent changes in $\overline{\rho'^2}$ exceed the mean-flow advection of density variance, more or less the situation envisioned by Andrews and McIntyre (1976). In the wind-forced case, near the surface the nonlinear influence of convective adjustment can contribute to the variance budget (Fig. 11a). Below the surface $\overline{\mathbf{u}'\rho'} \cdot \nabla\overline{\rho}$ is balanced by $\overline{\mathbf{u}} \cdot \nabla\overline{\rho'^2}/2$ around 1000-m depth, as suggested by McDougall and McIntosh (1996). Deeper in the ocean a combination of the triple eddy correlation term and the mean-flow advection of density variance balance $\overline{\mathbf{u}'\rho'} \cdot \nabla\overline{\rho}$. The diversity of possible balances and of our results indicates that G_z is unlikely to be easily parameterized.

An alternative to parameterizing G_z is to find a way to make it small by forcing $S(\mathbf{u}, \rho)$ to be nearly completely advective. We considered this alternative by seeking the optimal advective velocity $\mathbf{u}^*_{\text{opt}}$ required to minimize the diabatic component of (7) represented by G_z. This was done by finding the nondivergent $\mathbf{u}^*_{\text{opt}}$ that provided the least square error solution to $\mathbf{u}^*_{\text{opt}} \cdot \nabla\overline{\rho} = S(\mathbf{u}, \rho)$ and had no flow through the boundaries. The corresponding streamfunctions ψ^*_{opt} are shown in Figs. 6c and 7c. In neither case is ψ^*_{opt} aligned with isopycnals. For the Eady model, where G_z is smaller than the other advective terms at all depths, ψ^*_{opt} shown in Fig. 6c closely resembles ψ^* from the Andrews and McIntyre (1976) separation (8) and (9) shown in Fig. 6b. The wind-forced case shows less apparent correlation between the ψ^*_{opt} in Fig. 7c and ψ^* in Fig. 7b.

The results of these model analyses indicate that mesoscale eddies are a major factor controlling the large-scale density field. Not only are the adiabatic effects defined by $\mathbf{u}^* \cdot \nabla\overline{\rho}$ important, but the diabatic influence of G_z also matters. Thus, parameterizing both will be an important aspect of building a reliable time-evolving climate model. Since many existing subgrid-scale parameterizations (e.g., GM90; Visbeck et al. 1997) have been developed using the assumption that the cross-isopycnal advection represented by G_z is zero, the findings of this study suggest that further thought about basic parameterization requirements may be necessary in order to design models that evolve correctly in time.

5. Seeking an optimal subgrid-scale parameterization

The preceding section showed the significant influence of mesoscale processes on large-scale flow in both the baroclinically unsteady Eady problem and a wind-forced channel. In this section, we examine whether any commonly used subgrid-scale parameterizations can adequately represent the eddy-flux terms from the mesoscale models introduced in section 3. A perfect parameterization would allow the time evolution of coarse-

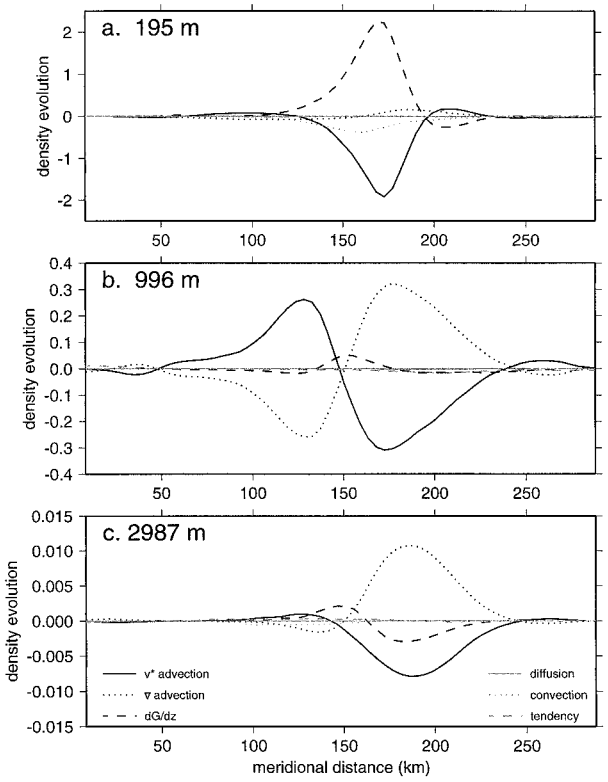

FIG. 9. Wind-forced model density balance (in kg m^{-3} s^{-1} $\times$ 10^5) zonally and time-averaged from model output at quarter-day intervals from day 3000 to 7000 for (a) level 4, (b) level 8, and (c) level 12. Terms of (7) are shown as in Fig. 8. Also included is the net influence of convective adjustment.

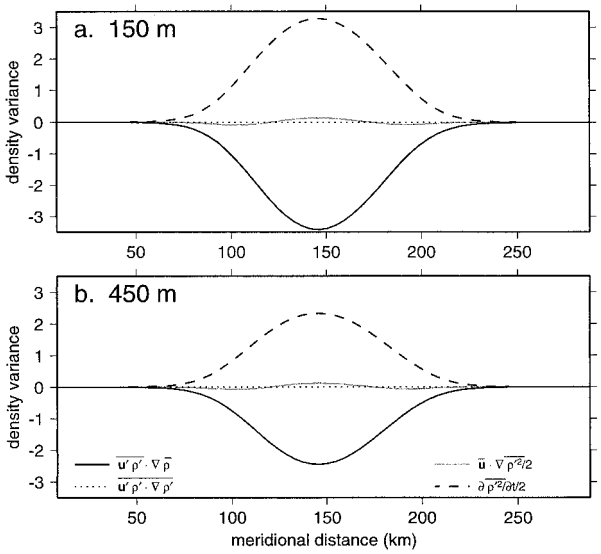

FIG. 10. Eady model density variance evolution as in (11) (in kg^2 m^{-6} s^{-1} $\times$ 10) averaged zonally and temporally for 15 model realizations from model snapshots at 5-day intervals from day 110 to 135 for (a) level 2 and (b) level 5. Terms represented are from (11) and show $\overline{p}_y\overline{v'\rho'} + \overline{w'\rho'}\overline{p}_z$ (black solid line); the eddy triple correlation term $\overline{(v'/2)\partial\rho'^2/\partial y} + \overline{(w'/2)\partial\rho'^2/\partial z}$ (black dotted line); advection of density variance by the mean flow $(\overline{v}/2)\partial\overline{\rho'^2}/\partial y + (\overline{w}/2)\partial\overline{\rho'^2}/\partial z$ (gray solid line); and the time evolution of density variance $\partial\overline{\rho'^2}/\partial t$ (gray dotted line). Friction and convective adjustment are negligible.

resolution model prognostic variables to track precisely the spatially filtered variables ($\overline{\mathbf{u}}$, $\overline{\rho}$) of a high-resolution model. A more modest goal is that the low-frequency part of a low-resolution model match the low-frequency, spatially filtered high-resolution model.

a. Diffusive parameterizations

One of the simplest subgrid-scale parameterizations is eddy diffusion, in which

$$-\overline{\mathbf{u}'\cdot\nabla\rho'} = K_H\nabla_H^2\overline{\rho} + K_v\frac{\partial^2\overline{\rho}}{\partial z^2}$$

$$= \text{horizontal} + \text{vertical diffusion}, \quad (12)$$

where ∇_H^2 is the horizontal Laplacian operator and K_H and K_v are constant horizontal and vertical eddy diffusion coefficients. Note the distinction between κ, which represents the diffusion coefficients set in the numerical models, and K, which represents the coefficient best estimated to represent the eddy flux as a diffusive process. In analogy with molecular diffusion, K_H and K_v should be positive. If they are not, diffusion creates local maxima, a process that is incompatible with the original physics.

Does (12) adequately represent the influence of mesoscale eddies? The time-averaged eddy-flux divergence terms on the left side of (12) are shown in Figs. 12a and 13a. For the Eady case, the horizontal Laplacian of the density fields in Fig. 12b is of opposite sign and has a slightly different spatial structure from the eddy-flux divergence terms. Similarly, in Fig. 13b, horizontal diffusion captures some of the large-scale structure of the time-averaged eddy fluxes. The vertical second derivatives of the density field in Figs. 12c and 13c are not closely related to the eddy-flux divergences.

For a quantitative comparison, we use a least squares fitting technique (see the appendix) to estimate optimal values of K_H and K_v. The effectiveness of the fit will be judged using the skill index Z, the percentage of the mean-squared eddy-flux divergence terms explained by the fit.

In addition to the diffusive parameterization in (12), we also consider a variety of other common parameterizations. Diffusion is often assumed to occur predominantly along isopycnals. Since density is constant along isopycnals, the isopycnal component of diffusion is zero, and (12) can be rewritten in terms of diapycnal diffusion:

$$-\overline{\mathbf{u}'\cdot\nabla\rho'} = K_d\frac{\partial^2\overline{\rho}}{\partial\eta^2} = \text{diapycnal diffusion}, \quad (13)$$

where η is perpendicular to isopycnal surfaces and K_d is the diapycnal diffusion coefficient.

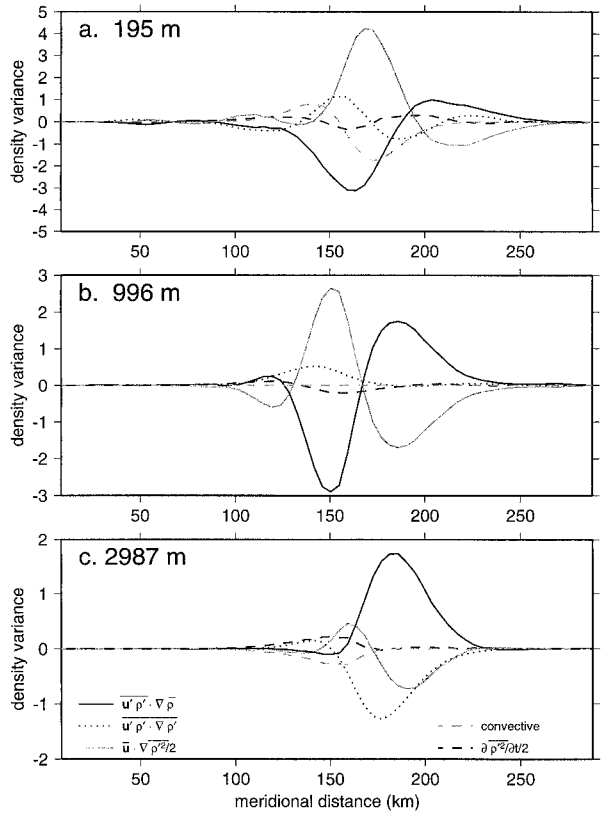

FIG. 11. Wind-forced model density variance (in kg^2 m^{-6} s^{-1}) zonally and time-averaged at quarter-day intervals from day 3000 to 7000 for (a) level 4, (b) level 8, and (c) level 12, which has been scaled up by 10^3. Terms represented are based on (11) as in Fig. 10, but convective adjustment (gray dashed line) is also included.

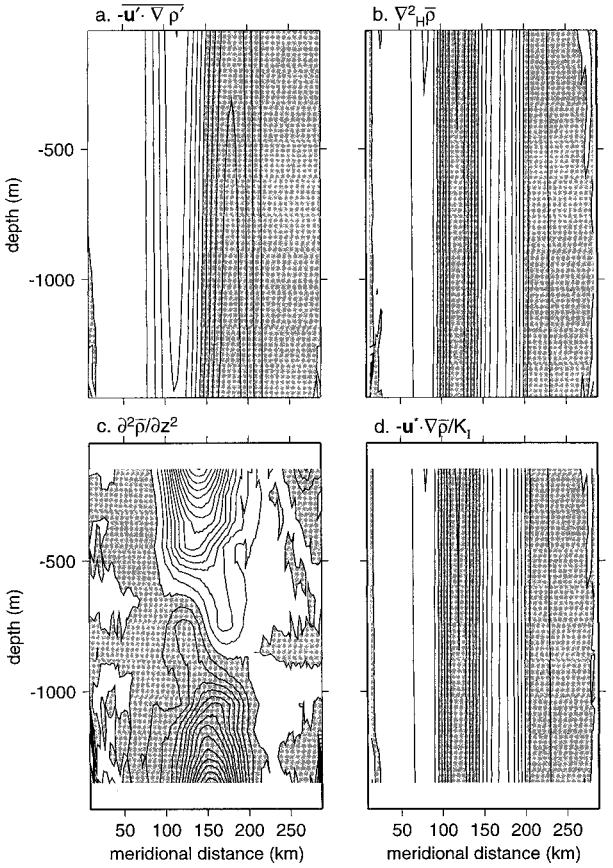

FIG. 12. Eddy flux divergences, diffusion terms (12), and GM90 parameterization (18) for the Eady instability case, averaged over 15 realizations and time-averaged from samples taken every 5 days from day 110 to day 135. Panels show (a) the eddy-flux divergence term $-\overline{\mathbf{u}' \cdot \boldsymbol{\nabla}\rho'}$ with contour interval 2.6×10^{-8} kg m^{-3} s^{-1}, (b) the horizontal eddy diffusion $\nabla_H^2\overline{\rho}$ with contour interval 3.7×10^{-12} kg m^{-5}, (c) the vertical eddy diffusion $\partial^2\overline{\rho}/\partial z^2$ with contour interval 1.9×10^{-8} in kg m^{-5}, and (d) $-\mathbf{u}^* \cdot \boldsymbol{\nabla}\overline{\rho}/K_I$ using the GM90 parameterization of $\mathbf{u}^*$, with contour interval 3.7×10^{-12} kg m^{-5}. Gray regions indicate negative values, and boundary values for the diffusion terms are not shown.

As an alternative to the constant vertical diffusion in (12), some numerical models have used a Richardson-number-dependent vertically varying value of K_v designed to respond to varying background stratification. As a proxy for that, we will also allow K_v to vary as a function of depth z:

$$-\overline{\mathbf{u}' \cdot \boldsymbol{\nabla}\rho'} = K_H\nabla_H^2\overline{\rho} + \frac{\partial}{\partial z}\left[K_v(z)\frac{\partial\overline{\rho}}{\partial z}\right]$$
$$= \text{horizontal} + \text{varying vertical diffusion}. \quad (14)$$

In analogy with (13), we also consider a depth-varying diapycnal diffusion in which K_d varies with depth:

$$-\overline{\mathbf{u}' \cdot \boldsymbol{\nabla}\rho'} = \frac{\partial}{\partial\eta}\left[K_d(z)\frac{\partial\overline{\rho}}{\partial\eta}\right]$$
$$= \text{vertically varying diapycnal diffusion}. \quad (15)$$

In place of diffusion, some investigators have confined eddy effects to higher wavenumbers by using biharmonic diffusion:

$$-\overline{\mathbf{u}' \cdot \boldsymbol{\nabla}\rho'} = A_H\nabla_H^4\overline{\rho} + K_v\frac{\partial^2\overline{\rho}}{\partial z^2}$$
$$= \text{biharmonic} + \text{vertical diffusion} \quad (16)$$

(e.g., Semtner 1986). We fit for A_H, the biharmonic diffusion coefficient, which should be negative for numerically stable downgradient diffusion, and K_v, the vertical diffusion coefficient.

Finally, we test the quasi-adiabatic GM90 parameterization in which the eddy-induced transport velocity $\mathbf{u}^*$ represented in (8) is parameterized directly:

$$\overline{\mathbf{u}' \cdot \boldsymbol{\nabla}\rho'} = \mathbf{u}^*_{\text{GM}} \cdot \boldsymbol{\nabla}\overline{\rho} = \text{GM90 parameterization} \quad (17)$$

with

$$\mathbf{u}^*_{\text{GM}} = \left[\left(K_I\frac{\overline{\rho}_x}{\overline{\rho}_z}\right)_z, \left(K_I\frac{\overline{\rho}_y}{\overline{\rho}_z}\right)_z, -\boldsymbol{\nabla}_H \cdot \left(K_I\frac{\nabla\overline{\rho}}{\overline{\rho}_z}\right)\right], \quad (18)$$

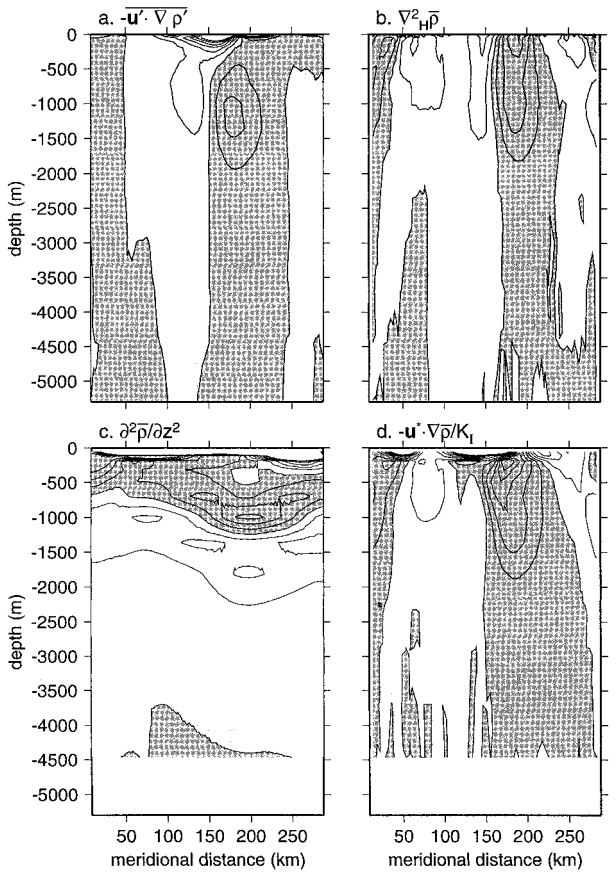

FIG. 13. Terms in (12) and (18) for the wind-forced model, time-averaged from samples taken every quarter-day from day 3000 to day 7000. As in Fig. 12, results show (a) $-\overline{\mathbf{u}' \cdot \nabla \rho'}$ with contour interval 5.0×10^{-7} kg m^{-3} s^{-1}, (b) $\nabla_H^2 \overline{\rho}$ with contour interval 1.4×10^{-9} kg m^{-5}, (c) $\partial^2 \overline{\rho}/\partial z^2$ with contour interval 7.1×10^{-5} kg m^{-5}, and (d) $-\mathbf{u}^* \cdot \nabla \overline{\rho}/K_I$ using the GM90 parameterization of $\mathbf{u}^*$ with contour interval 1.4×10^{-9} kg m^{-5}.

where K_I has the units of a diffusion coefficient. As in (8), $\mathbf{u}^*_{\rm GM}$ is by definition nondivergent. Danabasoglu et al. (1994) and McWilliams and Gent (1994) have implemented this parameterization to show substantial improvements in the ability of coarse-resolution models to simulate large-scale aspects of the general circulation.

Estimates of the meridional streamfunction $\psi^*_{\rm GM} = -K_I \overline{\rho}_y / \overline{\rho}_z$ corresponding to $\mathbf{u}^*_{\rm GM}$ are shown in Figs. 6d and 7d. Like the other streamfunctions shown in Figs. 6 and 7, the GM90 streamfunction is not directed along isopycnals. In addition, in neither case is there a close spatial similarity between $\psi^*_{\rm GM}$ and either ψ^*, the zonal average of the eddy-induced transport streamfunction from (8) (Figs. 6b and 7b), or $\psi^*_{\rm opt}$, the streamfunction that most nearly describes $\overline{\mathbf{u}' \cdot \nabla \rho'}$ (Figs. 6c and 7c), indicating that the parameterization does not capture the full advective processes.

The GM90 parameterization for the advective terms $\mathbf{u}^*_{\rm GM} \cdot \nabla \overline{\rho}/K_I$ is shown in Figs. 12d and 13d. In the Eady instability case, there is a close resemblance between the spatial structures of the GM90 parameterization terms (Fig. 12d) and of the horizontal diffusion terms (Fig. 12b). This is not surprising since the GM90 parameterization and horizontal diffusion are indistinguishable to leading order in Rossby number when standard quasigeostrophic scalings are applied. In the wind-forced case (Figs. 13b, d), the fields do not resemble each other as closely but show the same large-scale features.

In addition to the GM90 parameterization, we have also considered a variation proposed by Visbeck et al. (1997) that draws on ideas outlined by Green (1970) and Stone (1972) to predict the spatial structure of K_I. For a zonally averaged scenario, they suggest

$$K_I = \alpha \frac{|\overline{\rho}_y|}{\overline{\rho}_z} N l^2, \tag{19}$$

where α is constant and l is a characteristic length scale over which particles are transferred. In regions of small growth rate, l is determined by the Rossby radius; where the growth rate is larger, l increases to approach the width of the high-growth rate region.

We evaluate the success of these parameterizations at representing the zonal and time-averaged eddy-flux divergences in section 5b. In section 5c we assess the effectiveness of the parameterizations at representing the model output when less averaging is allowed.

b. Parameterization results

For each of the parameterizations, we sought coefficients K, A, or α that minimized the least square error in Eqs. (12)–(17) for time-averaged and zonally averaged fields. For the Eady case, presented in Table 2, time snapshots spaced at 5-day intervals from day 110 to 135 were averaged, and fits were calculated for each of 15 model realizations. Table 3 shows least squares fits of the various parameterizations of $\overline{\mathbf{u}' \cdot \nabla \rho'}$ sampled at quarter-day intervals and time-averaged over 4000 days for the wind-forced case.

For the Eady instability, the fraction Z of mean-squared $\overline{\mathbf{u}' \cdot \nabla \rho'}$ explained by the least squares fit approaches 60%, its largest value, for horizontal diffusion, GM90, and the Visbeck et al. (1997) parameterization. However, as we might have anticipated from Fig. 12, all three of these parameterizations produce diffusion coefficients of the wrong sign. Negative coefficients K and α imply that eddies tend to concentrate tracer distributions into narrower regions. In a practical model implementation, using diffusion coefficients to achieve upgradient density transfers is unstable and will lead to unphysical model behavior. Thus, if we constrain ourselves to stable positive values of K, for Eady's prototypical example of baroclinic instability, the instantaneous effects of eddies are diametrically different from both horizontal diffusion and from the GM90 parameterization, which was designed to represent instability. For the other Eady examples, Z is less than 1%, indi-

TABLE 2. Eady model fits for K, A, and α calculated for time-averaged model output sampled at 5-day intervals from day 110 to 135. Mean coefficients and uncertainties are based on 15 model runs. Values of K and A are in MKS units. The quantity Z and its standard deviation, here expressed as percentages, represent the fraction of the mean-squared flux divergence, $(\overline{\mathbf{u}' \cdot \nabla \rho'})^2$ explained by the parameterization (see appendix). Vertically varying cases are not included for the Eady model, since the small derivatives of the vertical density shear make the calculations unreliable.

Case	Coefficient	Mean best fit	Uncertainty	Z
Horizontal + vertical diffusion	K_H	-5.5×10^{3}	5.9×10^{1}	57% ± 2%
	$K\nu$	6.1×10^{-2}	2.0×10^{-3}	
Diapycnal diffusion	K_d	2.6×10^{-1}	7.7×10^{-3}	0.8% ± 0.1%
Biharmonic + vertical diffusion	A_H	-1.8×10^{-16}	7.7×10^{-18}	0.8% ± 0.1%
	$K\nu$	2.6×10^{-1}	7.7×10^{-3}	
GM90	K_I	-5.5×10^{3}	5.9×10^{1}	57% ± 2%
Visbeck et al.	α	-8.2×10^{4}	7.7×10^{2}	57% ± 2%

cating that the least squares fits capture a negligibly small fraction of the eddy-flux divergence. The failure of the parameterizations to represent the average Eady instability is not surprising. Because the Eady instability has only a single growing mode, all eddies transfer density in the same direction, and an ensemble of eddies will not balance each other out to provide a net diffusive flux.

In the wind-forced time-averaged case, the most successful of the parameterizations shown in Table 3 are the quasi-adiabatic parameterizations based on GM90 and Visbeck et al. (1997). Both of these capture 43% ± 5% of the spatial variance in $\overline{\mathbf{u}' \cdot \nabla \rho'}$, substantially more than would be represented using horizontal and vertical diffusion or any of the other parameterizations. Not surprisingly, given the similarities between horizontal diffusion and the GM90 parameterizations, the coefficients K_I and K_H are nearly the same within error bars, and the increased skill in the GM90 case apparently comes from the improved relationship it allows between horizontal and vertical diffusion. These findings are consistent with those of Visbeck et al. (1997), who also found that horizontal diffusion was less successful than the GM90 parameterization or any of its variations.

Although one might hope to find universally valid diffusion coefficients, the best fits for the Eady instability and wind-forced cases differ by several orders of magnitude. As shown in both Tables 2 and 3, those parameters that are effective in describing the flux divergence are reasonably well determined. Uncertainty in the Eady case is particularly small because the growing instability is essentially deterministic in form, if not phase. Nonetheless, for the Eady problem, the fitted coefficients are not universal parameters: changing the background stratification by 30% results in substantially different coefficients.

Even for long time averages, the parameterizations are unable to capture the entire eddy-flux divergence. Although G_z is large in the upper ocean, below 300 m over 90% of the time-mean $\overline{\mathbf{u}' \cdot \nabla \rho'}$ is explained by $\mathbf{u}^* \cdot \nabla \overline{\rho}$, with $\mathbf{u}^*$ computed based on (8). In contrast, in the same depth range $\mathbf{u}^*_{\mathrm{GM}} \cdot \nabla \overline{\rho}$ can explain only about 40% of the time-mean $\overline{\mathbf{u}' \cdot \nabla \rho'}$. Thus, the parameterized $\mathbf{u}^*_{\mathrm{GM}}$ appears to model $\mathbf{u}^*$ incompletely, and this may explain why Z is as small as 40%.

c. *Parameterizing time-varying phenomena*

Subgrid-scale parameterizations are intended primarily to represent the spatially and temporally averaged effects of mesoscale eddies. An ideal parameterization would accurately duplicate the effects of eddies over small spatial and temporal scales. We now examine how well the parameterizations discussed above apply to shorter timescales. The Eady problem represents an evolution far from equilibrium, and averaging flux potentials over shorter intervals does not change the results. However, without changing the zonal averaging of the wind-forced case, we can vary the degree of temporal

TABLE 3. Wind-forced channel model fits for K, A, and α calculated by averaging over days 3000 to 7000 in the model run. Means and uncertainties are based on averages over eight blocks of 500 days that were treated as uncorrelated parameter estimates.

Case	Coefficient	Mean best fit	Uncertainty	Z
Horizontal + vertical diffusion	K_H	1.0×10^{2}	1.1×10^{1}	10% ± 2%
	$K\nu$	3.9×10^{-3}	7.4×10^{-4}	
Diapycnal diffusion	K_d	5.4×10^{-3}	7.1×10^{-4}	1.8% ± 1.1%
Horizontal + varying vertical diffusion	K_H	9.8×10^{1}	9.9×10^{0}	14.3% ± 1.6%
	$\langle K\nu\,(z)\rangle$	2.0×10^{-1}	3.9×10^{-2}	
Vertically varying diapycnal diffusion	$\langle K_d\,(z)\rangle$	1.2×10^{-2}	3.5×10^{-4}	6.2% ± 2.1%
Biharmoic + vertical diffusion	A_H	4.5×10^{-17}	1.6×10^{-17}	1.8% ± 1.1%
	$K\nu$	5.4×10^{-3}	7.1×10^{-4}	
GM90	K_I	1.4×10^{2}	3.5×10^{0}	43% ± 5%
Visbeck et al.	α	3.0×10^{3}	1.4×10^{2}	43% ± 5%

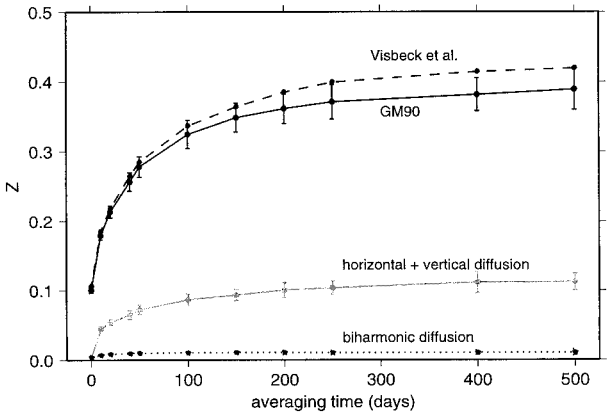

FIG. 14. The skill index Z as a function of averaging time, for days 3000 to 5000 of the wind-forced run for (gray line) horizontal and vertical diffusion, (dotted line) biharmonic diffusion, (solid line) GM90 parameterization, and (dashed line) Visbeck et al. (1997). Error bars represent standard deviations of Z divided by the square-root of the number of samples. Error bars for the Visbeck et al. case are approximately the same as GM90 error bars and are not shown.

averaging to see how the success of the parameterizations changes.

Figure 14 shows Z as a function of averaging time for horizontal diffusion, biharmonic diffusion, the GM90 parameterization, and the Visbeck et al. parameterization for the wind-forced case. Regardless of the parameterization selected, Z is small for short averaging times and asymptotes to its maximum value at long averaging times, with an e-folding scale of about 100 days. Over the shorter time periods indicated in Fig. 14, the density field undergoes greater variability, and eddy-flux divergences are less well represented by the parameterizations.

Ultimately the success of subgrid-scale parameterizations depends on the timescales of the processes studied. For this model, the frequency spectrum of density is red for time periods shorter than 200 days and then levels off. Apparently the parameterizations are most successful when applied to fields that have been averaged over time periods that are long compared with the decorrelation time of the detailed field. This suggests that parameterization of cases like the Eady problem may be effectively impossible because the average state evolves significantly over the the minimum averaging time required for parameterizations to be effective. For a system that has an inherently red frequency spectrum, without a low-frequency cutoff the minimum averaging time required for parameterizations to be effective may be too long to be useful.

For these model runs, parameterizations appear consistently better able to represent low-frequency effects than high-frequency fluctuations. Similarly in a different idealized model, Lee et al. (1997) found that only after many years of model integration did tracer distributions appear to be controlled by the eddy-induced advective velocity $\mathbf{u}^*$, which the GM90 parameterization is designed to represent. In a more realistic high-resolution North Atlantic model, Rix and Willebrand (1996) binned upper-ocean data into 4° boxes and temporally averaged over 19 years in order to obtain accurate statistical moments, but they did not consider the temporal evolution of their model. Their equivalent to Z, the squared correlation coefficient between $\mathbf{u}^*_{\mathrm{GM}}$ and $\mathbf{u}^*$ computed based on the eddy thickness flux, was between 38% and 52%, about the same as Z for the GM90 parameterization in Table 3.

A number of variations to the GM90 parameterization have been suggested but were not considered here. In these least squares fits, we avoided the domain boundaries where the second derivatives required for diffusion are ill-defined. However, Treguier et al. (1997) treated the eddy-flux divergence as diffusion of potential vorticity in the ocean interior and as diffusion of buoyancy at the boundaries; their analysis of the energetics and boundary requirements suggested constraints on the horizontal and vertical structure of the diffusivity. Killworth (1997) has also considered top and bottom boundary conditions along with the β effect, but in the simplified boundaryless f-plane examples used here, his parameterization is the same as the GM90 parameterization. Gent and McWilliams (1996) have argued that climate models would produce better results if the eddy-induced transport velocity $\mathbf{u}^*$ were also included in the momentum equations, but exploration of this effect is beyond the scope of the current study.

The results shown here do not offer definitive evaluations of eddy parameterizations for all possible situations. We have not included topography and the related physical process of form stress, which would alter the impact of mesoscale eddies and the corresponding eddy parameterizations. In addition, one might expect the dynamics of closed basins with clear continental boundaries to be somewhat different from the conceptually simple channel models examined in this paper. Finally, passive tracers, such as oxygen or nutrients, might show different types of eddy–mean flow interactions than the dynamically active density examined in this study and might have different parameterizations. What these results do show is that common parameterizations do not capture the instantaneous character of unstable eddies even when extensive zonal averaging is applied, but parameterizations that conserve the volume of water between isopycnal pairs, as suggested by GM90 or Visbeck et al. (1997), can sometimes credibly represent a portion of the time-averaged eddy-flux divergence.

6. Summary

Numerical models of slowly evolving climatic processes are typically run at coarse resolution and rely on parameterizations to represent the effects of mesoscale eddies. In this study two time-evolving model cases have been run in a zonal channel with sufficient resolution to examine the influence of mesoscale effects on

the larger scale. The first case, an Eady model, is unstable; the second, a wind-forced channel, evolves to a statistically steady state. The zonal average of the model variables was used to represent the coarse-resolution mean field, and the deviations from the zonal average were used to examine the influence of eddies on the mean density field. We specifically examined whether these eddy advective terms are adiabatic in the zonal mean (so that they conserve mean density) and whether they can be represented by any common eddy parameterizations.

The results show that eddy density fluxes dominate the zonal-mean density flux. Most eddy density advection neither creates nor destroys zonal-mean density. However a portion of the advection, G_z, is determined by the local deviations of the density field from the zonal-mean isopycnals, and at coarse resolution it appears diabatic. Thus, a reliable parameterization of subgrid-scale processes must account for the high-resolution eddy processes represented by G_z. As suggested by Tandon and Garrett (1996) these processes might include eddy diffusion over short length scales as well as interactions of small-scale features with the large-scale field. Although G_z can be determined from the variance budget, in the examples that we have considered, there is no simple dominant balance in the variance budget that might allow us to predict G_z.

Efforts to represent the eddy-flux processes using a number of common eddy parameterizations indicated that for averages over time periods long enough to filter out the most energetic fluctuations, the GM90 and Visbeck et al. (1997) parameterizations have skill indices of about 40%, in comparison with the 10% skill index of simple horizontal and vertical diffusion. Thus, for the modeling scenarios examined here, the quasi-adiabatic formulation suggested by GM90 is not perfect, but it represents an improvement over more traditional subgrid-scale parameterizations, for steady-state long-term model runs that do not depend on time-varying processes to represent any critical portion of their physics. In contrast, even with optimally selected diffusion coefficients, no parameterization reliably captures instantaneous or short time period eddy-induced processes.

Acknowledgments. Support for this work was provided by the National Oceanic and Atmospheric Administration (NOAA Award NA47GP0188 to the Lamont/Scripps Consortium for Climate Research.) Comments from Dan Rudnick and from the anonymous reviewers helped to improve the presentation.

APPENDIX

Fitting Diffusion Coefficients

In order to evaluate parameterizations like (12), spatially invariant coefficients K_H and K_v are determined by fitting the parameterizations to the zonally averaged eddy-flux terms $\overline{\mathbf{u}' \cdot \nabla \rho'}$. For the vertical–horizontal diffusion model (12) this leads to finding a least square misfit solution to

$$\mathbf{AK} = \begin{pmatrix} \nabla_H^2 \overline{\rho} & \dfrac{\partial^2 \overline{\rho}}{\partial z^2} \\ \vdots & \vdots \end{pmatrix} \begin{bmatrix} K_H \\ K_v \end{bmatrix} = \begin{pmatrix} \overline{\mathbf{u}' \cdot \nabla \rho'} \\ \vdots \end{pmatrix} = \mathbf{b}, \quad \text{(A1)}$$

where the elements of the matrix $\mathbf{A}$ are the horizontal and vertical Laplacians of $\overline{\rho}$ at all interior points in the model's zonally averaged y–z plane, and $\mathbf{b}$ contains the zonally averaged eddy-flux terms at the same y–z points. Only interior points are used because boundary values can dominate the least squares fit without being representative of domain-wide conditions. This is particularly true for the GM90 parameterization (Gent et al. 1995). Here $\mathbf{A}$ is column-weighted so that horizontal and vertical second derivatives of $\overline{\rho}$ have comparable influence on the solution.

A statistical measure of the results is the fraction of $\overline{\mathbf{u}' \cdot \nabla \rho'}$ explained, Z, which is closely related to the correlation of the eddy-flux terms to the model terms in $\mathbf{A}$:

$$Z = \text{fraction squared flux explained} = 1 - \frac{\overline{\left(Y - \sum_{i=1}^{M} K_i X_i\right)^2}}{\overline{Y^2}} = \frac{\overline{Y\tilde{Y}}}{\overline{Y^2}} = \frac{\overline{Y\tilde{Y}}^2}{\overline{Y^2}\,\overline{\tilde{Y}^2}}, \quad \text{(A2)}$$

where Y represents the observed eddy-flux terms $\overline{\mathbf{u}' \cdot \nabla \rho'}$, X_i are columns of $\mathbf{A}$ fit to Y with coefficients K_i, and $\tilde{Y}$ is the total functional fit. (If Y and $\tilde{Y}$ had zero mean, Z would be the correlation coefficient between Y and $\tilde{Y}$.) For comparison, if Y and X_i were statistically independent variables with zero mean and normal distribution, then the mean of Z would be M/N, where M is the number of parameters used in the fit (here 2) and N is the number of independent samples over which the fit is tested (here 780). Our data are correlated in time and space so estimating the effective value of N is difficult. In practice, the samples are not independent, and we expect Z to be greater than M/N.

To estimate the uncertainty in coefficients, we assume that the independently initialized Eady runs are statistically independent and that averages over 500-day segments of the wind-forced run are effectively independent. Thus, we can estimate the uncertainty of the average values from the variability. Standard error decreases as $1/\sqrt{P}$ where P is the number of assumed independent samples included in the average.

REFERENCES

Andrews, D. G., and M. E. McIntyre, 1976: Planetary waves in horizontal and vertical shear: The generalized Eliassen–Palm relation and the mean zonal acceleration. *J. Atmos. Sci.*, **33,** 2031–2048.

——, J. R. Holton, and C. B. Leovy, 1987: *Middle Atmosphere Dynamics.* Academic Press, 489 pp.
Bryan, K., S. Manabe, and R. C. Pacanowski, 1975: A global ocean–atmosphere climate model. Part II: The oceanic circulation. *J. Phys. Oceanogr.,* **5,** 30–46.
Cox, M. D., 1987: Isopycnal diffusion in a z-coordinate ocean model. *Ocean Modelling* (unpublished manuscript), **74,** 1–3.
Danabasoglu, G., and J. C. McWilliams, 1995: Sensitivity of the global ocean circulation to parameterizations of mesoscale tracer transports. *J. Climate,* **8,** 2967–2987.
——, ——, and P. R. Gent, 1994: The role of mesoscale tracer transports in the global ocean circulation. *Science,* **264,** 1123–1126.
Davis, R. E., 1994: Diapycnal mixing in the ocean: the Osborn-Cox model. *J. Phys. Oceanogr.,* **24,** 2560–2576.
Döös, K., and D. J. Webb, 1994: The Deacon Cell and the other meridional cells of the southern ocean. *J. Phys. Oceanogr.,* **24,** 429–442.
Eady, E. T., 1949: Long waves and cyclone waves. *Tellus,* **1** (3), 33–52.
FRAM Group, 1991: An eddy-resolving model of the southern ocean. *Eos, Trans. Amer. Geophys. Union,* **72,** 169–175.
Garner, S. T., N. Nakamura, and I. M. Held, 1992: Nonlinear equilibration of two-dimensional Eady waves: A new perspective. *J. Atmos. Sci.,* **49,** 1984–1996.
Gent, P. R., and J. C. McWilliams, 1990: Isopycnal mixing in ocean circulation models. *J. Phys. Oceanogr.,* **20,** 150–155.
——, and ——, 1996: Eliassen–Palm fluxes and the momentum equation in non-eddy-resolving ocean circulation models. *J. Phys. Oceanogr.,* **26,** 2540–2546.
——, J. Willebrand, T. J. McDougall, and J. C. McWilliams, 1995: Parameterizing eddy-induced tracer transports in ocean circulation models. *J. Phys. Oceanogr.,* **25,** 463–474.
Gill, A. E., 1982: *Atmosphere–Ocean Dynamics.* Academic Press, 662 pp.
Green, J. S. A., 1970: Transfer properties of the large-scale eddies and the general circulation of the atmosphere. *Quart. J. Roy. Meteor. Soc.,* **96,** 157–185.
Griffies, S. M., 1998: The Gent–McWilliams skew flux. *J. Phys. Oceanogr.,* **28,** 831–841.
Killworth, P. D., 1997: On the parameterization of eddy transfer. Part I: Theory. *J. Mar. Res.,* **55,** 1171–1197.
Lee, M. M., D. P. Marshall, and R. G. Williams, 1997: On the eddy transfer of tracers: Advective of diffusive? *J. Mar. Res.,* **55,** 1–24.
McDougall, T. J., and P. C. McIntosh, 1996: The temporal-residual-mean velocity. Part I: Derivation and the scalar conservation equations. *J. Phys. Oceanogr.,* **26,** 2653–2665.
McWilliams, J. C., and P. R. Gent, 1994: The wind-driven ocean circulation with an isopycnal thickness parameterization. *J. Phys. Oceanogr.,* **24,** 46–65.
——, G. Danabasoglu, and P. R. Gent, 1996: Tracer budgets in the warm water sphere. *Tellus,* **48A,** 179–192.
Osborn, T. R., and C. S. Cox, 1972: Oceanic fine structure. *Geophys. Fluid Dyn.,* **3,** 321–345.
Pacanowski, R. C., 1995: MOM 2 documentation user's guide and reference manual. GFDL Ocean Tech. Rep. 3, GFDL/NOAA, Princeton, NJ, 232 pp. [Available from GFDL/NOAA, P.O. Box 308, Princeton, NJ 08542-0308.]
Pedlosky, J., 1987: *Geophysical Fluid Dynamics.* 2d ed. Springer-Verlag, 710 pp.
Plumb, R. A., and J. D. Mahlman, 1987: The zonally averaged transport characteristics of the GFDL general circulation/transport model. *J. Atmos. Sci.,* **44,** 298–327.
Rix, N. H., and J. Willebrand, 1996: Parameterization of mesoscale eddies as inferred from a high-resolution circulation model. *J. Phys. Oceanogr.,* **26,** 2281–2285.
Samelson, R., 1993: Linear instability of a mixed-layer front. *J. Geophys. Res.,* **98,** 10 195–10 204.
Semtner, A. J., 1986: Finite-difference formulation of a world ocean model. *Proceedings of the NATO Advanced Physical Oceanographic Numerical Modelling.* J. J. O'Brien, Ed., D. Riedel, 187–202.
——, and R. M. Chervin, 1992: Ocean general circulation from a global eddy-resolving model. *J. Geophys. Res.,* **97,** 5493–5550.
Stone, P. H., 1972: A simplified radiative-dynamical model for the static stability of rotating atmospheres. *J. Atmos. Sci.,* **29,** 405–418.
Tandon, A., and C. Garrett, 1996: On a recent parameterization of mesoscale eddies. *J. Phys. Oceanogr.,* **26,** 406–411.
Treguier, A. M., I. M. Held, and V. D. Larichev, 1997: Parameterization of quasigeostrophic eddies in primitive equation models. *J. Phys. Oceanogr.,* **27,** 567–580.
Visbeck, M., J. Marshall, T. Haine, and M. Spall, 1997: On the specification of eddy transfer coefficients in coarse resolution ocean circulation models. *J. Phys. Oceanogr.,* **27,** 381–402.
Williams, G. P., 1971: Baroclinic annulus waves. *J. Fluid Mech.,* **49,** 417–449.